

## Durene-decorated CBP derivatives as phosphorescent hosts and exciton-blocking materials for efficient blue OLEDs†

Lijun Deng,<sup>a</sup> Xinzeng Wang,<sup>b</sup> Zhengchuan Zhang<sup>b</sup> and Jiuyan Li<sup>\*a</sup>

Received 6th June 2012, Accepted 1st August 2012

DOI: 10.1039/c2jm33636g

Two novel durene-containing molecules, 1,4-bis-[4-(9-carbazolyl)-phenyl]-durene (CPD) and 1,4-bis-{4-[9-(3,6-(di-*tert*-butyl)carbazoyl)]-phenyl}-durene (*t*-BuCPD), which are derived from 4,4'-bis(9-carbazolyl)biphenyl (CBP) by inserting durene in its biphenyl core, are designed and synthesized for use as host materials for blue phosphors in organic light-emitting diodes (OLEDs). Inserting durene in biphenyl causes a right-angle torsion between the durene and the adjacent phenyl groups due to the strong steric hindrance effect of the durene group, confining the effective  $\pi$ -conjugation on only one carbazole and one phenyl and increasing the triplet energies of CPD and *t*-BuCPD to over 3.0 eV. These durene-decorated molecules show higher thermal stabilities than many other CBP derivatives. Blue phosphorescent OLEDs were fabricated using CPD and *t*-BuCPD as triplet hosts and traditional iridium(III)bis(4,6-(difluorophenyl)pyridinato-N,C<sup>2'</sup>)picolinate (Firpic) as a dopant and excellent performances were achieved. In particular, peak efficiencies of 26.2 cd A<sup>-1</sup> and 14.8 lm W<sup>-1</sup> were realized when CPD was used as both a host and exciton-blocking material. This is the first report using durene to tune the triplet energy levels of phosphorescent host materials.

## 1. Introduction

There has been rapid growing interest in Ir<sup>III</sup>-based phosphorescent organic light-emitting diodes (PhOLEDs) because phosphorescent emitters can harvest both singlet and triplet excitons and achieve, in theory, 100% internal quantum efficiency.<sup>1,2</sup> However, since phosphorescence emitters generally have relatively long excited-state lifetimes, which could induce self-quenching at high concentrations, they are usually doped into a host.<sup>3,4</sup> In a host-dopant system, the dopant molecules usually get excited through two typical mechanisms: direct charge trapping and energy transfer from the host.<sup>5,6</sup> Direct charge trapping by the dopant only occurs when the lowest unoccupied molecular orbital (LUMO) of the dopant is lower than that of the host, and/or the highest occupied molecular orbital (HOMO) of the dopant is higher than that of the host.<sup>7-9</sup> For large band-gap blue-emitting phosphors, it is not as easy as green or red emitters to directly trap holes or electrons due to its relatively high LUMO level and low HOMO level.<sup>10,11</sup> Therefore, a significantly high triplet energy level of the host for blue phosphors is more important than for green and red emitters in order to guarantee efficient exothermic energy transfer from the excited host

molecules to the ground-state dopant ones.<sup>12,13</sup> At the same time, a significantly high triplet energy of the host is also necessary to prevent backward energy transfer from the dopant to the host and to effectively confine excitons on the dopant.<sup>14</sup> The ideal triplet energy ( $E_T$ ) between the singlet ground state ( $S_0$ ) and the triplet excited state ( $T_1$ ) for blue host materials should be at least 2.75 eV providing that the blue phosphor has a phosphorescence peak at 450 nm.<sup>15</sup>

Up to now, many attempts have been made to develop substances that have high triplet energies and are suitable host materials for blue phosphors in PhOLEDs.<sup>16-19</sup> The most successful blue hosts are the carbazole-based molecules due to the high intrinsic triplet energy of 3.0 eV for carbazole and their efficient hole transporting ability. One traditional example is polyvinylcarbazole (PVK), which has an  $E_T$  of 3.0 eV.<sup>20</sup> Based on the polymeric nature and high triplet energy, PVK is widely used as a universal host for solution-processed blue, green and red PhOLEDs.<sup>21</sup> However, PVK has a relatively low HOMO level (-5.8 eV). As a result, PVK-containing OLEDs usually have relatively high driving voltages due to a large hole injection barrier in the anode-PVK interface.<sup>22</sup> *N,N'*-Dicarbazolyl-3,5-benzene (mCP) is one small molecular blue host material that is widely used in vacuum deposited PhOLEDs.<sup>6</sup> The *meta*-linkage of the two carbazoles over the phenyl ring in mCP confines the effective conjugation of the whole molecule on only one carbazole and one phenyl, resulting in a high  $E_T$  of 2.9 eV. A maximum external electroluminescent quantum efficiency of 7.5% and a luminous power efficiency of 8.9 lm W<sup>-1</sup> were

<sup>a</sup>State Key Laboratory of Fine Chemicals, School of Chemical Engineering, Dalian University of Technology, 2 Linggong Road, Dalian 116024, China. E-mail: jiuyanli@dlut.edu.cn; Fax: +86 411 84986233

<sup>b</sup>School of Chemistry, Dalian University of Technology, 2 Linggong Road, Dalian 116024, China

† Electronic supplementary information (ESI) available. See DOI: 10.1039/c2jm33636g

obtained for devices based on mCP and Firpic. However, the low molecular weight of mCP results in a low glass transition temperature ( $T_g$ ) of 60 °C and high crystallinity, which are definitely not favorable for OLED stability. In addition to PVK and mCP, the derivatives of 4,4'-bis(9-carbazolyl)-biphenyl (CBP) are another typical series of blue phosphorescent host materials.<sup>5</sup> In CBP, the molecular structure allows for extended conjugation of the carbazole units over the biphenyl core leading to a decrease of  $E_T$  to around 2.56 eV.<sup>5</sup> Although CBP has sometimes been used as a host for blue phosphors, e.g. iridium(III)bis(4,6-(difluorophenyl)pyridinato-N,C<sup>2'</sup>)picolinate (Firpic), the device performance has been limited due to the endothermic forward energy transfer from the CBP host to the blue phosphor and an unavoidable reverse energy transfer from the dopant to the host. Therefore, structural modification of CBP has been intensively performed with the aim of increasing the triplet energy to afford a blue host. One typical CBP derivative, which has been used as a blue host, is 4,4'-bis(9-carbazolyl)-2,2'-dimethylbiphenyl (CDBP),<sup>23</sup> in which the biphenyl is forced into a tilted conformation due to the steric effect of two methyl groups and, consequently, the triplet energy is increased to 3.0 eV due to reduced molecular conjugation. The OLED based on CDBP and Firpic exhibited a current efficiency of 20.5 cd A<sup>-1</sup> and a power efficiency of 10.5 lm W<sup>-1</sup>. In a similar way, a trifluoromethyl substituent was also introduced into the 2,2'-positions of the biphenyl ring to design blue host materials with high  $E_T$  values.<sup>24,25</sup> The other type of CBP-based blue host incorporates non-conjugated units, such as aliphatic cyclobutyl ring,<sup>26</sup> an oxygen bridge,<sup>27</sup> or a diphenylsilane linker<sup>28</sup> inserted within the biphenyl core. The presence of these non-conjugated units confines the effective conjugation to only a half length of CBP, resulting in high  $E_T$  values. Another group of CBP derivatives is the CBP isomers, which are obtained by varying the linkage of two carbazoles at the *meta*- or *ortho*-positions of the central biphenyl core to form *m*-CBP or *o*-CBP, instead of the *para*-linkage in CBP.<sup>29</sup> In this way, the conjugation of each carbazole is spread over only the phenyl ring that it is directly bound to, rather than to the biphenyl core or the whole molecule. Therefore, the  $E_T$  of these two CBP isomers are tuned to 3.0 eV for *o*-CBP and 2.84 eV for *m*-CBP. Excellent performances with high efficiencies of 29.9 cd A<sup>-1</sup> and 14.4 lm W<sup>-1</sup> were obtained for blue PhOLEDs using these CBP isomers as phosphorescent hosts, which represented the highest efficiency so far for Firpic-based blue OLEDs using CBP derivatives as phosphorescent hosts. It is clear that the reason for the increase in the  $E_T$  values for all the aforementioned strategies, such as using a short linking bridge in PVK and mCP, varying the linkage topology in *m*-CBP and *o*-CBP, incorporating bulky groups with steric hindrance in CDBP and introducing non-conjugated units, is to minimize the effective conjugation length of carbazoles with unsaturated moieties.

In this work, we report the design and synthesis of two novel CBP derivatives, 1,4-bis-[4-(9-carbazolyl)-phenyl]-durene (CPD) and 1,4-bis-[4-[9-(3,6-(di-*tert*-butyl)carbazolyl)]-phenyl]-durene (*t*-BuCPD) (Scheme 1), for use as host materials for blue phosphors in OLEDs. Durene was selected as the key building block and was inserted in between the biphenyl group of CBP with the expectation that the multiple methyl groups on durene may cause strong steric hindrance and interrupt the conjugation of the

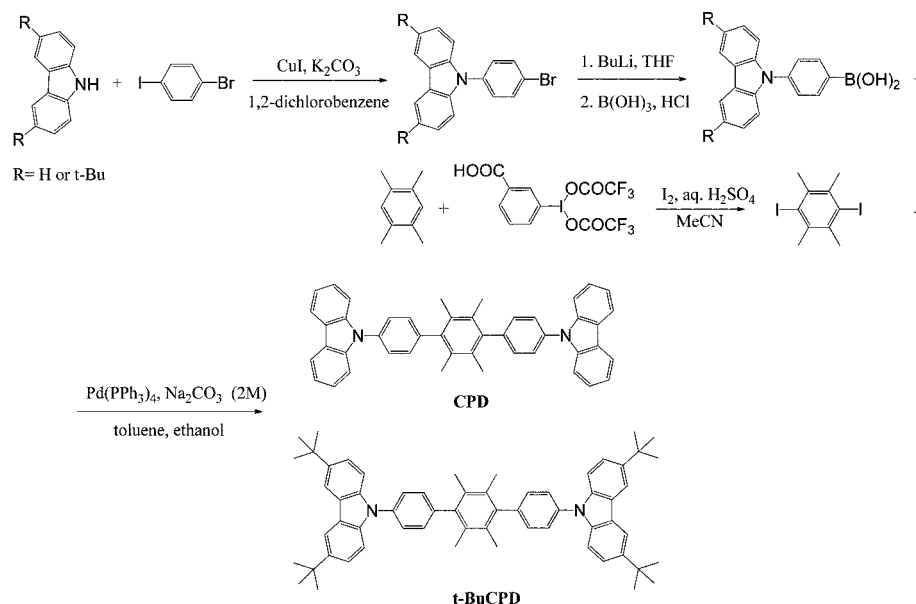
whole molecule. Therefore, high triplet energies may be possible for these novel CBP derivatives. CPD and *t*-BuCPD designed in this way possess excellent thermal stabilities ( $T_d = 463$  °C and 450 °C) (better than most other CBP derivatives) and high  $E_T$  values of over 3.0 eV. Blue phosphorescent OLEDs containing CPD and *t*-BuCPD as hosts and Firpic as a dopant exhibited excellent performance. In particular, peak efficiencies of 26.2 cd A<sup>-1</sup> and 14.8 lm W<sup>-1</sup> were realized when CPD was used as both a host and an exciton-blocking material. As far as we know, this is the first report using durene to tune the triplet energy levels of phosphorescent host materials.

## 2. Results and discussion

### 2.1 Synthesis and thermal properties

The chemical structures and detailed synthetic protocol of CPD and *t*-BuCPD are shown in Scheme 1. Both of them are synthesized through a Suzuki cross-coupling reaction between 1,4-diiododurene and the corresponding carbazole-containing boronic acid.<sup>30</sup> The common intermediate, 1,4-diiododurene, was prepared by the oxidative iodination of durene with 3-[bis(trifluoroacetoxy)iodo]benzoic acid at a high isolation yield of 80%.<sup>31</sup> The corresponding carbazole-containing boronic acid intermediates were prepared following the procedure described in Scheme 1.<sup>32</sup> First, the 4-(9-carbazolyl)-1-bromo-benzene was prepared by selective coupling of carbazole with 1-bromo-4-iodobenzene in the presence of cuprous iodide under the Ullmann condensation conditions. The corresponding 4-(9-carbazolyl)-1-phenylboronic acid was then easily obtained by treatment of 4-(9-carbazolyl)-1-bromo-benzene with *n*-butyl lithium at a low temperature, followed by reaction with trimethyl borate at room temperature and subsequently acid hydrolysis. The palladium-catalyzed Suzuki cross-coupling of excess 4-(9-carbazolyl)-1-phenylboronic acid or 4-[9-(3,6-(di-*tert*-butyl)carbazolyl)]-1-phenylboronic acid with 1,4-diiododurene generated the desired product, CPD, in a high yield of 85% or *t*-BuCPD in a yield of 80%. All the intermediates and target products were soluble and adequately stable in common organic solvents, such as dichloromethane, making it possible to purify them by silica-gel column chromatography. All of them were fully characterized by <sup>1</sup>H and <sup>13</sup>C NMR, mass spectrometry, and elemental analysis.

The thermal properties of the CPD and *t*-BuCPD were examined by thermogravimetric analysis (TGA) and differential scanning calorimetry (DSC) in a nitrogen atmosphere at a scanning rate of 10 K min<sup>-1</sup>. All related data are listed in Table 1. As shown in Fig. 1, both materials show high thermal stabilities with an onset of weight loss ( $T_D$ ) at 463 °C and 450 °C, which are far above those of CBP (365 °C), CDBP (310 °C), *o*-CBP (317 °C) and *m*-CBP (411 °C). The high thermal stabilities of these two molecules may result from the presence of the durene moiety. When a CPD powder was heated for the DSC measurement, only an endothermic transition at 374 °C was detected, which was assigned to the melting of CPD. Other phase transitions, including the glass transition were not observed under the present conditions even after the melted sample was rapidly cooled and reheated for a second run. For *t*-BuCPD, melting was not observed. However, a melting point of 374 °C

Scheme 1 Synthetic route to CPD and *t*-BuCPD.

for CPD is still higher than those of CBP and other CBP derivatives, also implying the improved thermal stability that is caused by the durene group.

## 2.2 Optical and electrochemical properties

The UV-vis absorption and photoluminescence (PL) spectra of CPD and *t*-BuCPD were measured in  $\text{CH}_2\text{Cl}_2$ . The spectra are shown in Fig. 2a and all pertinent data are summarized in Table 1. For comparison, the spectra of CBP was measured under identical conditions and is provided in Fig. 2a as well. Compounds CPD and *t*-BuCPD show very similar absorption profiles that contain two major absorption bands. For CPD, the absorption at 293 nm can be assigned to the  $\pi-\pi^*$  absorption of the carbazole-centered units, which is identical to that of CBP. Whereas the weak absorption in the range of 320 nm to 350 nm can be attributed to  $\pi-\pi^*$  transitions of the conjugated structure between the carbazole unit and its adjacent phenyl unit in the molecule. This assignment can be confirmed by the fact that the intensity of this band is significantly reduced in comparison with that of CBP, which could be ascribed to the decreased  $\pi$ -conjugation in CDP due to the introduction of the bulky durene group. However, the additional *tert*-butyl substituents on the 3,6-positions of the carbazole ring cause a bathochromic shift in the

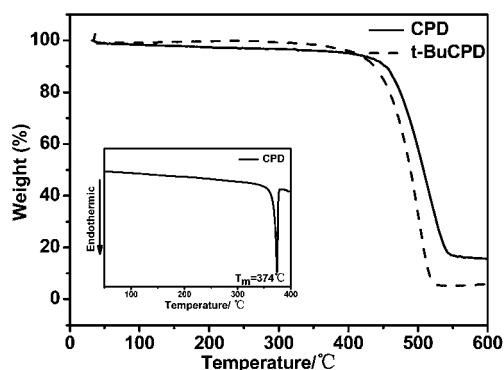


Fig. 1 TGA thermograms of CPD and *t*-BuCPD. Inset: the DSC trace of CPD.

absorption spectrum by 4–6 nm for *t*-BuCPD in comparison with CPD. Upon photoexcitation, CPD emits violet fluorescence with a peak at 351 nm and a shoulder at 364 nm. For compound *t*-BuCPD, the same fluorescence spectral profile was obtained and a similar bathochromic shift of 9 nm was observed in its fluorescence spectrum as in the absorption spectrum in comparison with CPD. There have been similar reports that decoration of carbazole rings at the 3,6-positions with methyl substituents for

Table 1 Physical data of CPD, *t*-BuCPD and CBP

Compound	$T_D^a$ [°C]	$T_m^b$ [°C]	$\lambda_{\text{abs}}$ [nm] in $\text{CH}_2\text{Cl}_2$	$\lambda_{\text{em}}$ [nm] in $\text{CH}_2\text{Cl}_2$	$E_g^c$ [eV]	$E_{\text{ox}}^{\text{onset}d}$ [V]	HOMO/LUMO $^e$ [eV]	$E_T^f$ [eV]
CPD	463	374	293, 328, 342	351, 364(s) <sup>h</sup>	3.52	1.23	-5.63/-2.11	3.02
<i>t</i> -BuCPD	450	No. <sup>g</sup>	297, 334, 348	360, 372(s) <sup>h</sup>	3.47	1.08	-5.48/-2.01	3.00
CBP	365	283	293, 319	379	3.42	1.29	-5.69/-2.27	2.67

<sup>a</sup>  $T_D$  is the thermal decomposition temperature in a thermogravimetric experiment at a heating rate of 10 K min<sup>-1</sup> in a nitrogen atmosphere. <sup>b</sup>  $T_m$  is the melting temperature. <sup>c</sup> The optical band gap estimated from the absorption edge ( $\lambda_{\text{edge}}$ ) of a solid film by the equation:  $E_g = 1240/\lambda_{\text{edge}}$ . <sup>d</sup> vs. the saturated calomel electrode (SCE). <sup>e</sup> HOMO (eV) =  $-e(4.4 + E_{\text{ox}}^{\text{onset}})$ , LUMO (eV) = HOMO +  $E_g$ . <sup>f</sup>  $E_T$ , the triplet energy, estimated from the highest energy vibronic sub-band of the phosphorescence spectra. <sup>g</sup> No. = Not obtained. <sup>h</sup> s = Shoulder.

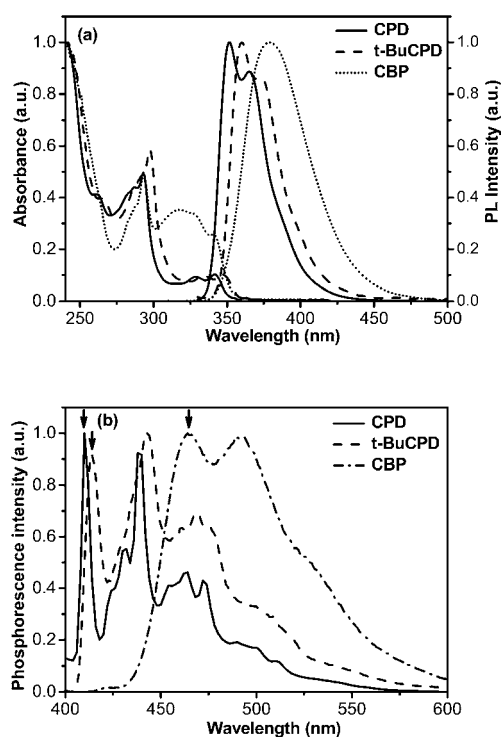


**Fig. 2** (a) UV-vis absorption and PL spectra of CPD, *t*-BuCPD and CBP in dilute CH<sub>2</sub>Cl<sub>2</sub> at 293 K and (b) phosphorescence spectra of these compounds at 77 K in 2-Me-THF. The arrows indicate the inferred triplet level positions.

other CBP derivatives results in a bathochromic shift of both the absorption and fluorescence spectra.<sup>24</sup> In contrast to the fine vibronic structure of CPD and *t*-BuCPD, CBP exhibits a structureless fluorescence spectrum under identical conditions with an emission peak at 379 nm. It is obvious that inserting durene in between the biphenyl core of the CBP molecule causes a large blue shift of the fluorescence by 28 nm for CPD, which could be ascribed to the decreased  $\pi$ -conjugation in CPD due to the strong steric hindrance of the durene group.

As a prerequisite for host materials, the triplet energy should be higher than that of the phosphorescent emitter. The phosphorescence spectra of CPD, *t*-BuCPD and CBP were measured in frozen 2-Me-THF solutions at a low temperature and illustrated in Fig. 2b and their triplet energies were determined from the highest energy peak of the phosphorescence spectra. CPD and *t*-BuCPD reach triplet energies of *ca.* 3.02 and 3.0 eV, respectively, being much higher than 2.67 eV for CBP. Apparently, the insertion of durene in biphenyl causes a hypsochromic shift of the

phosphorescence, generating a high triplet energy of over 3.0 eV and assuring that these durene-decorated CBP derivatives are suitable host materials for blue phosphorescent emitters.

The electrochemical properties of CPD and *t*-BuCPD were measured by cyclic voltammetry in deoxygenated CH<sub>2</sub>Cl<sub>2</sub> containing 0.1 M tetra(*n*-butyl)ammonium hexafluorophosphate (*n*-Bu<sub>4</sub>NPF<sub>6</sub>) as a supporting electrolyte. The cyclic voltammograms are shown in Fig. 3. During the anodic scan, CPD exhibits the irreversible oxidation wave with an onset potential ( $E_{\text{ox}}^{\text{onset}}$ ) at 1.23 V vs. saturated calomel electrode (SCE), which can be assigned to the oxidation of the carbazole units. It should be noted that one additional sharp peak was observed at about 0.8 V in the reduction process. This additional reduction peak has been frequently observed for other non-protected carbazole derivatives<sup>29</sup> and was attributed to the instability of the radical cations of the carbazole moiety.<sup>24</sup> In contrast to CPD, with the introduction of *tert*-butyl groups at the 3,6-positions of the carbazoles, *t*-BuCPD exhibits a reversible oxidation wave. The absence of the additional sharp peak for *t*-BuCPD confirms that the electrochemical stability of the carbazole moiety was improved by adding protecting groups at its 3,6-positions. Moreover, the electron-donating *tert*-butyl groups<sup>24,33</sup> shift the oxidation of *t*-BuCPD to a slightly more positive potential than CPD, with  $E_{\text{ox}}^{\text{onset}}$  at 1.08 V vs. SCE. The HOMO levels for CPD and *t*-BuCPD are calculated as 5.63 and 5.48 eV, respectively, according to the equation  $E_{\text{HOMO}} = -e(E_{\text{onset}}^{\text{ox}} + 4.4)$ . The LUMO levels are determined as 2.10 eV and 2.02 eV, respectively, according to  $E_{\text{LUMO}} = E_{\text{HOMO}} + E_{\text{g}}$  (where  $E_{\text{g}}$  is the optical energy gap obtained from the absorption threshold of film samples).<sup>34,35</sup> In comparison with parent CBP, both the HOMO and LUMO of CPD and *t*-BuCPD are slightly increased to higher levels. However, the larger rise of the LUMO with regards to the HOMO resulted in an increased HOMO-LUMO

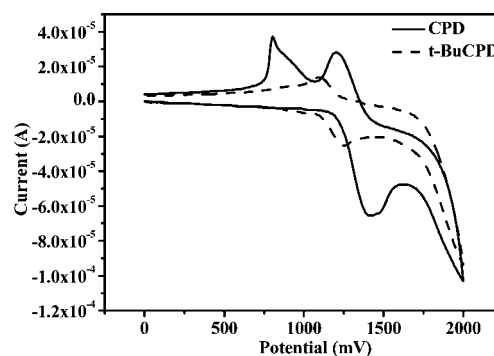


**Fig. 3** Cyclic voltammograms of CPD and *t*-BuCPD.

**Table 2** EL performance data of the blue OLEDs with CPD, *t*-BuCPD and mCP as hosts

Device	Host	$V_{\text{on}}$ [V]	$L_{\text{max}}^a$ [cd m <sup>-2</sup> ]	$\eta_{\text{L}}^a$ [cd A <sup>-1</sup> ]	$\eta_{\text{L}}^b$ [cd A <sup>-1</sup> ]	$\eta_{\text{p}}^a$ [lm W <sup>-1</sup> ]	$\eta_{\text{ex.}}$ (%) <sup>a</sup>	CIE (x, y) at 10 V
A	CPD	5.0	16 580 (12)	18.5 (8)	12.0	8.3 (7)	8.7	(0.18, 0.43)
B	<i>t</i> -BuCPD	9.0	3760 (20)	5.8 (11)	7.2	1.7 (11)	2.4	(0.17, 0.39)
C	mCP	6.8	14 860 (14)	14.5 (8)	8.7	5.7 (8)	6.7	(0.18, 0.41)
D	CPD	5.0	11 130 (12)	26.2 (6)	9.0	14.8 (5)	10.0	(0.19, 0.45)
E	<i>t</i> -BuCPD	7.0	6693 (15)	18.0 (8)	6.6	8.0 (7)	7.5	(0.18, 0.41)

<sup>a</sup> The maximum values of the devices. The data in parentheses are the voltages (V) at which these data were obtained. <sup>b</sup> At 100 mA cm<sup>-2</sup>.

energy gap for these derivatives, which is consistent with their higher triplet energies in comparison to CBP.

### 2.3 Theoretical calculations

In order to understand how the inserted durene affects the molecular configuration and the excited state energies, density functional theory (DFT) calculations were performed for CPD and *t*-BuCPD using B3LYP hybrid functional theory with Gaussian 03.<sup>36</sup> The structure of CBP was also optimized under identical conditions for comparison. Fig. 4 illustrates the geometry optimized structures of CPD, *t*-BuCPD and CBP. For CBP, the two phenyl rings align with each other by a small torsion angle of 36°. With insertion of durene in between these two phenyl rings in CPD, a large torsion angle of 90° was formed between each phenyl and the durene ring owing to the steric hindrance effect of durene. This indicates that the electron clouds of each phenyl ring almost have no interaction with those of the neighbouring durene ring, due to the right-angle torsion of these six-member rings, and the presence of durene completely breaks the  $\pi$ -electron conjugation of the molecule. In a similar way, the presence of durene causes a large torsion angle of 87° between the phenyl and the durene ring in *t*-BuCPD. However, the spatial alignment of the peripheral carbazoles with their adjacent phenyl rings does not show obvious variation in these molecules, with torsion angles ranging from 52° to 55°. Evidently, the right-angle torsion between durene and the adjacent phenyl rings and the subsequent broken  $\pi$ -conjugation fully account for the increased HOMO–LUMO energy gaps and the higher triplet energies for these durene-containing molecules.

The HOMO and LUMO distribution for CPD, *t*-BuCPD and CBP are shown in Fig. 5. For CBP, the HOMO is distributed over the whole molecule, including the central biphenyl and the external carbazole rings, while the LUMO is localized on the biphenyl moiety. With insertion of durene in the biphenyl, the HOMOs of both CPD and *t*-BuCPD spread mainly onto the external carbazole rings, with tiny contribution from the phenyl rings. At the same time, the LUMOs of both CPD and *t*-BuCPD shift completely to the carbazole rings from the original biphenyl core of CBP. Notably, the durene moiety does not contribute to either the HOMO or LUMO for both molecules since it has no effective conjugation with any adjacent groups, which are responsible for the high triplet energies of these durene-based molecules.

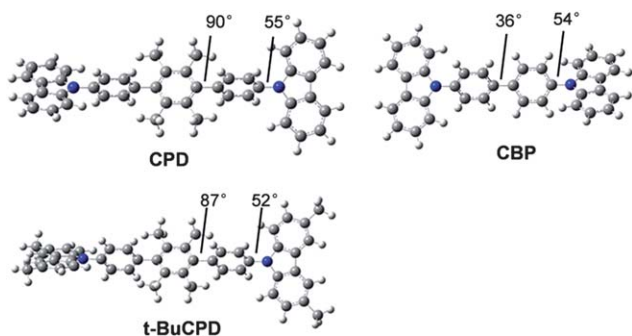


Fig. 4 Geometry optimized structures of CBP, CPD and *t*-BuCPD. The torsion angles are indicated in the figure.

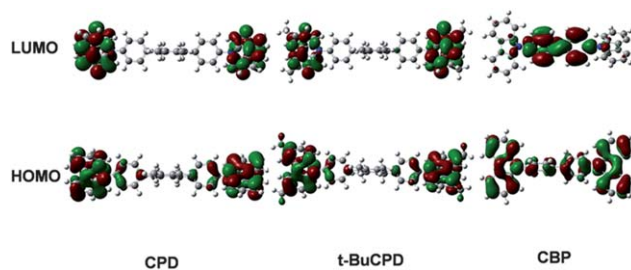


Fig. 5 Contour plots of the frontier molecular orbitals of CPD, *t*-BuCPD and CBP in the ground state.

### 2.4 Phosphorescent OLEDs

In order to evaluate the electroluminescent properties of these novel durene-based CBP derivatives, blue phosphorescent OLEDs were fabricated by the vacuum evaporation technique using Firpic as a dopant and CPD or *t*-BuCPD as the host in the emitting layer. These OLEDs have the configuration of ITO/PEDOT : PSS (40 nm)/NPB (20 nm)/host : Firpic (10 wt%, 30 nm)/TPBI (40 nm)/LiF (1 nm)/Al (150 nm) (host = CPD: device A; host = *t*-BuCPD: device B), in which PEDOT : PSS is poly(3,4-ethylenedioxythiophene) : poly(styrenesulfonate) and acts as a hole-injecting layer, NPB is *N,N'*-bis(naphthalene-1-yl)-2,2'-dimethylbiphenyl and acts as hole-transporting layer, TPBI is 2,2',2''-(1,3,5-benzinetriyl)-tris(1-phenyl-1*H*-benzimidazole) and acts as electron-transporting and hole-blocking layer. For comparison, traditional mCP was also used as a host to fabricate the control device C, which has an identical configuration to devices A and B. mCP was selected as the host of the control device mainly because it is the most widely used host material for blue phosphorescent OLEDs to date. Since our durene-based CPD and *t*-BuCPD and the dimethyl-based CDBP are all based on the same strategy of disturbing conjugation to increase the triplet energy, we also fabricated another control device (F) with an identical configuration to device A but with CDBP as the host. A comparison of the performance for the CDBP and CPD devices is provided in Fig. S1 of the ESI.† At a doping concentration of 10 wt%, all these devices exhibited blue electroluminescence from the Firpic molecules without residual emission from the hosts or the adjacent layers. This is likely to be due to the significant high triplet energy of CPD and *t*-BuCPD, which guarantees efficient forward energy transfer from the host to the dopant and effectively confines triplet excitons on the dopant molecules.

Fig. 6a shows the current density–voltage characteristics of these OLEDs. It is obvious that the CPD-based device A has a much lower driving voltage than *t*-BuCPD-based device B and mCP-based device C. For example, at a given voltage of 10 V, devices A, B and C exhibit current densities of 46, 0.13 and 5 mA cm<sup>-2</sup>, respectively. The much lower driving voltage of CPD-based device A in comparison with mCP-based device C may be ascribed to the more efficient hole injection in device A. As illustrated by the energy level diagram in Fig. 7, the electron injection barrier at the host–TPBI interface is 0.59, 0.69 and 0.4 eV for devices A, B and C, respectively, all of which are much higher than the negative electron injection barrier (−0.3 eV) from TPBI to the Firpic dopant. Therefore, direct electron trapping by

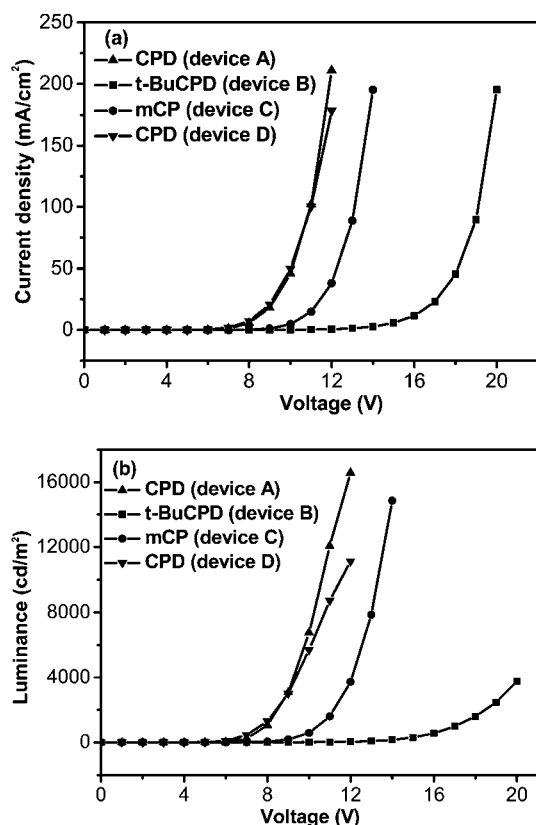


Fig. 6 The current density–voltage ( $J$ – $V$ ) curves (a) and the luminance–voltage ( $L$ – $V$ ) characteristics (b) of OLEDs A, B, C and D.

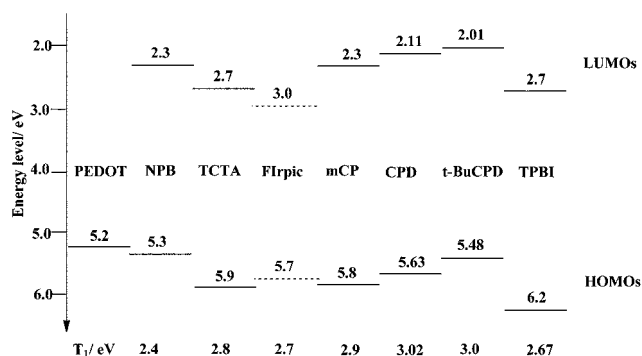


Fig. 7 Energy level alignment of all active materials used in the OLEDs of the present study.

the Firpic molecules will dominate the major electron injection process at the TPBI–host interface and the electron injection process will be very efficient in all these three devices regardless of the different LUMO levels of these three hosts. However, the hole injection efficiency at the NPB–host interface is determined by the HOMO levels of the hosts. The hole injection from NPB to the host is the major factor to determine the hole injection since direct hole trapping by the Firpic dopant is impossible due to its too low HOMO ( $-5.7$  eV). The hole injection barrier from NPB to CPD and to mCP are 0.33 and 0.5 eV, respectively, implying that hole injection in CPD-based device A is more efficient than in mCP-based device C. Evidently, the relatively high HOMO

level of CPD and, thus, the easier hole injection, accounts for the lower driving voltage of CPD-based device A in comparison to mCP-based device C. On the other hand, *t*-BuCPD has a similar HOMO level to CPD, while the *t*-BuCPD-based device B has higher driving voltages than device A. This may be because *t*-BuCPD probably possesses lower hole drift mobility than CPD due to the presence of saturated *tert*-butyl groups. This deduction can be manifested by the higher current density in the single carrier devices of CPD in comparison with *t*-BuCPD. As depicted in Fig. 8, both the hole-only devices, ITO/NPB (30 nm)/CPD or *t*-BuCPD (30 nm)/Al (150 nm), and the electron-only devices, ITO/TPBI (30 nm)/CPD or *t*-BuCPD (30 nm)/TPBI (30 nm)/LiF (1 nm)/Al (150 nm), of CPD exhibit significantly higher currents than those of *t*-BuCPD, indicating that the presence of the *tert*-butyl groups in *t*-BuCPD is not favorable for both hole and electron transportation. This is reasonable since the saturated *tert*-butyl groups are not only redox non-active, but also prevent the orderly stacking of the molecules and the efficient charge carrier transportations. The bulk mobility-depending feature of device B can be further confirmed by the less oblique  $J$ – $V$  curve of device B at a higher electrical field region with regards to device A.

In line with the  $J$ – $V$  characteristics, the luminance–voltage ( $L$ – $V$ ) curves of devices A, B and C follow a similar order in terms of their driving voltage, as shown in Fig. 6b. CPD-based device A exhibited good performance with a maximum brightness of  $16\,580\text{ cd m}^{-2}$  at 12 V, which is much higher than that of mCP-based device C ( $14\,860\text{ cd m}^{-2}$  at 14 V). A peak luminance efficiency of  $18.5\text{ cd A}^{-1}$  (Fig. 9), corresponding to a power efficiency of  $8.3\text{ lm W}^{-1}$ , was obtained for device A, which is also slightly higher than that of device C ( $14.5\text{ cd A}^{-1}$ , corresponding to  $5.7\text{ lm W}^{-1}$ ). The detailed performance data of these devices are compared in Table 2. Apparently, the durene-containing CPD exhibited better performance than traditional mCP when used as a blue phosphorescent host material in OLEDs. As shown in Fig. S1 of the ESI†, under an identical device configuration, CPD-based device A also exhibited a better performance in comparison to the CDBP-based control device F, with a decreased driving voltage and slightly enhanced brightness and efficiency.

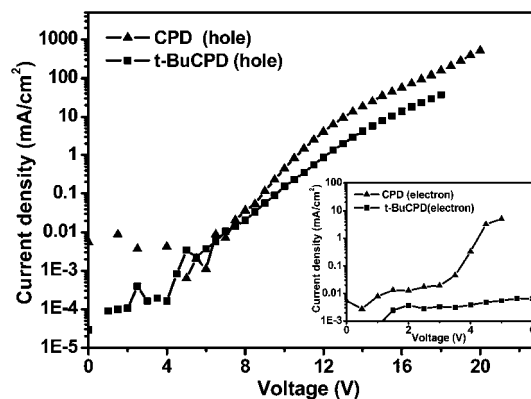


Fig. 8 The current density–voltage ( $J$ – $V$ ) curves for the hole-only devices (ITO/NPB (30 nm)/CPD or *t*-BuCPD (30 nm)/Al (150 nm)). Inset: the  $J$ – $V$  curves for electron-only devices (ITO/TPBI (30 nm)/CPD or *t*-BuCPD (30 nm)/TPBI (30 nm)/LiF (1 nm)/Al (150 nm)).

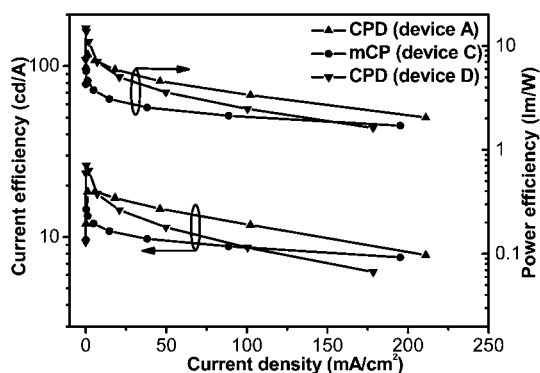


Fig. 9 Plots of the current efficiency versus the current density for devices A, C and D.

It should be noted that in devices A, B and C, it is still possible for the electrogenerated triplet excitons of the Firpic molecules to be quenched by NPB in the neighbouring layer, which has lower a triplet energy (2.4 eV), although the high triplet energy of the host can prevent backward energy transfer to the host molecules. A similar exciton quenching behaviour of dopant molecules by low-energy materials in the adjacent layer has been reported for other systems.<sup>14,37</sup> Therefore, in order to optimize the device performance of device A, a thin layer (10 nm) of neat CPD was inserted in between NPB and the emitting layer to act as an exciton blocking layer owing to its high triplet energy to form device D. The structure of device D is ITO/PEDOT : PSS (40 nm)/NPB (20 nm)/CPD (10 nm)/CPD : Firpic (10 wt%, 30 nm)/TPBI (40 nm)/LiF (1 nm)/Al (150 nm). The current density and luminance of device D are shown in Fig. 6a and b, respectively. It is clear that the presence of this additional 10 nm CPD layer did not bring obvious changes to the current density and brightness of device D in comparison to device A. However, the efficiency of device D is significantly increased to  $26.2 \text{ cd A}^{-1}$  (Fig. 9), which is much higher than the maximum value of  $18.2 \text{ cd A}^{-1}$  for device A. The remarkably enhanced efficiency of device D, especially in the low-driving voltage range, fully confirms the exciton blocking function of the CPD layer.

For optimization of *t*-BuCPD-based device B, device E was fabricated by introducing 4,4',4''-tris-(*N*-carbazolyl)-triphenylamine (TCTA) as an exciton blocking layer. The structure of device E is ITO/PEDOT : PSS (40 nm)/NPB (20 nm)/TCTA (10 nm)/*t*-BuCPD : Firpic (10 wt%, 30 nm)/TPBI (40 nm)/LiF (1 nm)/Al (150 nm). TCTA was selected as the exciton blocking layer rather than *t*-BuCPD itself, because of its good hole-transporting ability along with its high triplet energy. As expected, the performance of device E was much improved in comparison to B, with a maximum brightness of  $6693 \text{ cd m}^{-2}$  at 15 V, a maximum luminance efficiency of  $18.0 \text{ cd A}^{-1}$  and a peak power efficiency of  $8.0 \text{ lm W}^{-1}$ . The performance of all above devices are summarized in Table 2. The enhanced performance of devices D and E proved that it is essential to confine the triplet excitons in the emitting layer to improve the device efficiency.

### 3. Conclusions

In conclusion, two novel durene-based CBP derivatives, CPD and *t*-BuCPD, have been developed for use as host materials in

phosphorescent OLEDs. We have demonstrated that inserting durene between the two phenyl rings of CBP greatly increases the triplet energy of the molecules to over 3.0 eV since the steric hindrance effect of durene causes right-angle torsion, which results in a break of the conjugation. As a result, the traditional green and red phosphorescent CBP host was successfully transformed into a blue phosphorescent host. In addition, this design strategy endows these materials with high thermal stability. Excellent performance was achieved when these CBP derivatives were used as hosts for blue-emitting phosphors in OLEDs. A high efficiency of  $26.2 \text{ cd A}^{-1}$  ( $14.8 \text{ lm W}^{-1}$ ) was realized when CPD was employed as both the host and an exciton-blocking material. It was also observed that the presence of saturated *tert*-butyl groups in the *t*-BuCPD molecule is not favorable for charge transportation. Considering the easy synthesis and performance advantages, these durene-based CBP derivatives, especially CPD, are promising host materials for applications in highly efficient and stable blue phosphorescent OLEDs.

## 4. Experimental

### General information

<sup>1</sup>H NMR and <sup>13</sup>C NMR spectra were recorded on a 400 MHz and 100 MHz Varian Unity Inova spectrophotometer. Mass spectra were taken on MALDI micro MX and HP1100LC/MSD MS spectrometers. The photoluminescence and UV-vis absorption spectral measurements were performed on a Perkin-Elmer LS55 spectrometer and a Perkin-Elmer Lambda 35 spectrophotometer, respectively. Phosphorescence spectra were measured on an Edinburgh FLS920 spectrometer at 77 K in 2-Me-THF.

The electrochemical measurements of CPD and *t*-BuCPD were carried out by using a conventional three-electrode configuration and an electrochemical workstation (BAS100B, USA) at a scan rate of  $100 \text{ mV s}^{-1}$ . A glass carbon working electrode, a Pt-wire counter electrode and a saturated calomel electrode (SCE) reference were used. All measurements were made at room temperature on samples dissolved in dichloromethane, deoxygenated with argon, and with 0.1 M  $[\text{Bu}_4\text{N}]\text{PF}_6$  as the electrolyte.

Density functional theory (DFT) calculations using B3LYP functional were performed. The basis set used for the C, H, N atoms was 6-31 G. There are no imaginary frequencies for the optimized structures. All these calculations were performed with the Gaussian 03 package.<sup>36</sup>

### OLED fabrication and measurements

Pre-cleaned ITO glass substrates with a sheet resistance of  $30 \Omega \square^{-1}$  were treated with UV-ozone for 20 min. A 40 nm thick PEDOT : PSS film was first deposited on the ITO glass substrates and baked at  $120 \text{ }^\circ\text{C}$  for 30 min in air. Then, a 20 nm thick NPB was vacuum deposited on the PEDOT : PSS film. The subsequent organic layers were deposited sequentially under a base pressure less than  $10^{-6}$  torr in a vacuum chamber. For all the OLEDs, the emitting layers were deposited by co-evaporation of Firpic and the corresponding host. The emitting area of each pixel was determined by the overlap of two electrodes as  $9 \text{ mm}^2$ . The EL spectra, CIE coordinates and *L-V-J* curves of the devices were measured with a PR705 photometer and a

source-measure-unit Keithley 236 under ambient conditions at room temperature.

### Syntheses of compounds

All reagents and solvents were obtained from Aldrich, Acros or the Energy Chemical Co. and the solvents were treated as required prior to use. Commercially available reagents were used without further purification unless otherwise stated. All reactions were performed under a nitrogen atmosphere. The important intermediates, including 4-(9-carbazolyl)-1-phenylboronic acid, 4-[9-(3,6-(di-*tert*-butyl)carbazolyl)]-1-phenylboronic acid,<sup>32</sup> 1,4-diiododurene<sup>31</sup> and the reference compound CDBP,<sup>23</sup> were synthesized and characterized according to the literature methods.

*General procedure for the preparation of 1,4-bis-[4-(9-carbazolyl)-phenyl]-durene (CPD) and 1,4-bis-{4-[9-(3,6-(di-*tert*-butyl)carbazolyl)]-phenyl}-durene (*t*-BuCPD):* a mixture of 1,4-diiododurene (385.9 mg, 1 mmol), 4-(9-carbazolyl)-1-phenylboronic acid or 4-[9-(3,6-(di-*tert*-butyl)carbazolyl)]-1-phenylboronic acid (2.5 mmol), tetrakis(triphenylphosphine) palladium(0) (69.3 mg, 0.06 mmol), 2 M potassium carbonate (2 mL), toluene (20 mL) and ethanol (4 mL) was stirred under an atmosphere of nitrogen at 80 °C for 6 h. After cooling to room temperature, the reaction mixture was poured into cool water and extracted with dichloromethane (3 × 50 mL). The combined organic layers were dried over anhydrous sodium sulfate, filtered and evaporated to dryness. The crude product was then purified by silica gel column chromatography with light petroleum : dichloromethane = 10 : 1 as an eluent to afford the pure product as a white solid.

CPD: Yield 85%. <sup>1</sup>H NMR (400 MHz, CDCl<sub>3</sub>) δ (ppm): 2.13 (s, 12H, CH<sub>3</sub>), 7.31–7.35 (t, 4H, Ar), 7.45–7.49 (t, 8H, Ar), 7.54–7.56 (d, 4H, Ar), 7.66–7.68 (d, 4H, Ar), 8.18–8.20 (d, 4H, Ar). <sup>13</sup>C NMR (100 MHz, CDCl<sub>3</sub>): 142.0, 141.0, 140.7, 136.0, 132.2, 130.9, 127.0, 125.9, 123.4, 120.3, 119.9, 109.8, 18.37. MALDI-TOF-MS (*m/z*): 616.1 [M]<sup>+</sup>. Anal. Calcd. For C<sub>46</sub>H<sub>36</sub>N<sub>2</sub>: C, 89.58; H, 5.88; N, 4.54%. Found: C, 89.46; H, 5.92; N, 4.58%.

*t*-BuCPD: Yield 80%. <sup>1</sup>H NMR (400 MHz, CDCl<sub>3</sub>) δ (ppm): 1.49 (s, 36H, CH<sub>3</sub>), 2.11 (s, 12H, CH<sub>3</sub>), 7.41–7.43 (d, 4H, Ar), 7.48–7.53 (m, 8H, Ar), 7.64–7.66 (d, 4H, Ar), 8.18 (s, 4H, Ar). <sup>13</sup>C NMR (100 MHz, CDCl<sub>3</sub>): 142.8, 141.4, 140.7, 139.2, 136.4, 132.1, 130.8, 126.5, 123.6, 123.3, 116.2, 109.3, 34.7, 32.0, 18.3. MALDI-TOF-MS (*m/z*): 840.5 [M]<sup>+</sup>. Anal. Calcd. For C<sub>62</sub>H<sub>68</sub>N<sub>2</sub>: C, 88.52; H, 8.15; N, 3.33%. Found: C, 88.47; H, 8.20; N, 3.39%.

### Acknowledgements

We thank the National Natural Science Foundation of China (21072026 and 20923006), the Ministry of Education for the New Century Excellent Talents in University (Grant NCET-08-0074), the NKBRFSF (2009CB220009) and the Fundamental Research Funds for the Central Universities (DUT12ZD211) for the financial support of this work.

### References

- (a) M. A. Baldo, D. F. O'Brian, Y. You, A. Shoustikov, S. Sibley, M. E. Thompson and S. R. Forrest, *Nature*, 1998, **395**, 151; (b)

- S. Lamansky, P. Djurovich, D. Murphy, F. Abdel-Razzaq, H.-E. Lee, C. Adachi, P. E. Burrows, S. R. Forrest and M. E. Thompson, *J. Am. Chem. Soc.*, 2001, **123**, 4304.
- (a) C. Ulbricht, B. Beyer, C. Friebe, A. Winter and U. S. Schubert, *Adv. Mater.*, 2009, **21**, 4418; (b) Y. You and S. Y. Park, *J. Am. Chem. Soc.*, 2005, **127**, 12438.
- (a) Y. Tao, Q. Wang, C. Yang, Q. Wang, Z. Zhang, T. Zou, J. Qin and D. Ma, *Angew. Chem., Int. Ed.*, 2008, **47**, 8104; (b) S. Reineke, F. Linder, G. Schwartz, N. Seidler, K. Walzer, B. Lüssem and K. Leo, *Nature*, 2009, **459**, 234; (c) R. Wang, D. Liu, H. Ren, T. Zhang, H. Yin, G. Liu and J. Li, *Adv. Mater.*, 2011, **23**, 2823.
- (a) S.-J. Su, H. Sasabe, T. Takeda and J. Kido, *Chem. Mater.*, 2008, **20**, 1691; (b) J. Zou, H. Wu, C.-S. Lam, C. Wang, J. Zhu, C. Zhong, S. Hu, C.-L. Ho, G.-J. Zhou, H. Wu, W. C. H. Choy, J. Peng, Y. Cao and W.-Y. Wong, *Adv. Mater.*, 2011, **23**, 2976; (c) R. Wang, D. Liu, R. Zhang, L. Deng and J. Li, *J. Mater. Chem.*, 2012, **22**, 1411.
- C. Adachi, R. C. Kwong, P. Djurovich, V. Adamovich, M. A. Baldo, M. E. Thompson and S. R. Forrest, *Appl. Phys. Lett.*, 2001, **79**, 2082.
- R. J. Holmes, S. R. Forrest, Y.-J. Tung, R. C. Kwong, J. J. Brown, S. Garon and M. E. Thompson, *Appl. Phys. Lett.*, 2003, **82**, 2422.
- C.-H. Fan, P. Sun, T.-H. Su and C.-H. Cheng, *Adv. Mater.*, 2011, **23**, 2981.
- W.-S. Huang, J. T. Lin and H.-C. Lin, *Org. Electron.*, 2008, **9**, 557.
- Y.-L. Chang, Z. B. Wang, M. G. Helander, J. Qiu, D. P. Puzzo and Z. H. Lu, *Org. Electron.*, 2012, **13**, 925.
- L. Chen, H. You, C. Yang, D. Ma and J. Qin, *Chem. Commun.*, 2007, 1352.
- S. O. Jeon, S. E. Jang, H. S. Son and J. Y. Lee, *Adv. Mater.*, 2011, **23**, 1436.
- C.-H. Yang, Y.-M. Cheng, Y. Chi, C.-J. Hsu, F.-C. Fang, K.-T. Wong, P.-T. Chou, C.-H. Chang, M.-H. Tsai and C.-C. Wu, *Angew. Chem., Int. Ed.*, 2007, **46**, 2418.
- M.-F. Wu, S.-J. Yeh, C.-T. Chen, H. Murayama, T. Tsuboi, W.-S. Li, I. Chao, S.-W. Liu and J.-K. Wang, *Adv. Funct. Mater.*, 2007, **17**, 1887.
- Y. Tao, Q. Wang, C. Yang, C. Zhong, J. Qin and D. Ma, *Adv. Funct. Mater.*, 2010, **20**, 2923.
- L. Xiao, Z. Chen, B. Qu, J. Luo, S. Kong, Q. Gong and J. Kido, *Adv. Mater.*, 2011, **23**, 926.
- G. T. Lei, L. D. Wang, L. Duan, J. H. Wang and Y. Qiu, *Synth. Met.*, 2004, **144**, 249.
- S. O. Jeon and J. Y. Lee, *J. Mater. Chem.*, 2012, **22**, 7239.
- M.-H. Tsai, Y.-H. Hong, C.-H. Chang, H.-C. Su, C.-C. Wu, A. Matoliukstyte, J. Simokaitiene, S. Grigalevicius, J. V. Grazulevicius and C.-P. Hsu, *Adv. Mater.*, 2007, **19**, 862.
- P.-I. Shih, C.-L. Chiang, A. K. Dixit, C.-K. Chen, M.-C. Yuan, R.-Y. Lee, C.-T. Chen, E. W.-G. Diau and C.-F. Shu, *Org. Lett.*, 2006, **8**, 2799.
- M. J. Yang and T. Tsutsui, *Jpn. J. Appl. Phys.*, 2000, **39**, L828.
- K. S. Yook, S. E. Jang, S. O. Jeon and J. Y. Lee, *Adv. Mater.*, 2010, **22**, 4479.
- P. Zacharias, M. C. Gather, M. Rojahn, O. Nuyken and K. Meerholz, *Angew. Chem., Int. Ed.*, 2007, **46**, 4388.
- S. Tokito, T. Iijima, Y. Suzuki, H. Kita, T. Tsuzuki and F. Sato, *Appl. Phys. Lett.*, 2003, **83**, 569.
- P. Schrögel, A. Tomkeviciene, P. Strohriegel, S. T. Hoffmann, Anna Köhler and C. Lennartz, *J. Mater. Chem.*, 2011, **21**, 2266.
- S. T. Hoffmann, P. Schrögel, M. Rothmann, R. Q. Albuquerque, P. Strohriegel and A. Köhler, *J. Phys. Chem. B*, 2011, **115**, 414.
- D. R. Whang, Y. You, S. H. Kim, W.-I. Jeong, Y.-S. Park, J.-J. Kim and S. Y. Park, *Appl. Phys. Lett.*, 2007, **91**, 233501.
- J. He, H. Liu, Y. Dai, X. Ou, J. Wang, S. Tao, X. Zhang, P. Wang and D. Ma, *J. Phys. Chem. C*, 2009, **113**, 6761.
- D. Hu, P. Lu, C. Wang, H. Liu, H. Wang, Z. Wang, T. Fei, X. Gu and Y. Ma, *J. Mater. Chem.*, 2009, **19**, 6143.
- S. Gong, X. He, Y. Chen, Z. Jiang, C. Zhong, D. Ma, J. Qin and C. Yang, *J. Mater. Chem.*, 2012, **22**, 2894.
- Y. Liu, X. Xu, F. Zheng and Y. Cui, *Angew. Chem., Int. Ed.*, 2008, **47**, 4538.
- M. S. Yusubov, T. V. Funk, K.-W. Chi, E.-H. Cha, G. H. Kim, A. Kirschning and V. V. Zhdankin, *J. Org. Chem.*, 2008, **73**, 295.
- M. J. Xiong, Z. H. Li and M. S. Wong, *Aust. J. Chem.*, 2007, **60**, 603.
- P. Schrögel, N. Langer, C. Schildknecht, G. Wagenblast, C. Lennartz and P. Strohriegel, *Org. Electron.*, 2011, **12**, 2047.

- 
- 34 B. Liang, L. Wang, Y. Xu, H. Shi and Y. Cao, *Adv. Funct. Mater.*, 2007, **17**, 3580.
- 35 P. E. Burrows, Z. Shen, V. Bulovic, D. M. McCarty and S. R. Forrest, *J. Appl. Phys.*, 1996, **79**, 7991.
- 36 M. J. Frisch, *et al.*, *Gaussian 03 (Revision C.02)*, Gaussian, Inc., Wallingford CT, 2004.
- 37 S.-J. Lee, J.-H. Seo, J.-H. Kim, H.-M. Kim, K.-H. Lee, S.-S. Yoon and Y.-K. Kim, *Thin Solid Films*, 2010, **518**, 6184.